Editors' Suggestion

Signatures of Quark-Hadron Phase Transitions in General-Relativistic Neutron-Star Mergers

Elias R. Most,[1] L. Jens Papenfort,[1] Veronica Dexheimer,[2] Matthias Hanauske,[1,3] Stefan Schramm,[1,3] Horst Stöcker,[1,3,4] and Luciano Rezzolla[1,3]

[1]*Institut für Theoretische Physik, Max-von-Laue-Straße 1, 60438 Frankfurt, Germany*
[2]*Department of Physics, Kent State University, Kent, Ohio 44243, USA*
[3]*Frankfurt Institute for Advanced Studies, Ruth-Moufang-Straße 1, 60438 Frankfurt, Germany*
[4]*GSI Helmholtzzentrum für Schwerionenforschung GmbH, 64291 Darmstadt, Germany*

(Received 10 July 2018; revised manuscript received 7 October 2018; published 12 February 2019)

Merging binaries of neutron-stars are not only strong sources of gravitational waves, but also have the potential of revealing states of matter at densities and temperatures not accessible in laboratories. A crucial and long-standing question in this context is whether quarks are deconfined as a result of the dramatic increase in density and temperature following the merger. We present the first fully general-relativistic simulations of merging neutron-stars including quarks at finite temperatures that can be switched off consistently in the equation of state. Within our approach, we can determine clearly what signatures a quark-hadron phase transition would leave in the gravitational-wave signal. We show that if after the merger the conditions are met for a phase transition to take place at several times nuclear saturation density, they would lead to a postmerger signal considerably different from the one expected from the inspiral, that can only probe the hadronic part of the equations of state, and to an anticipated collapse of the merged object. We also show that the phase transition leads to a very hot and dense quark core that, when it collapses to a black hole, produces a ringdown signal different from the hadronic one. Finally, in analogy with what is done in heavy-ion collisions, we use the evolution of the temperature and density in the merger remnant to illustrate the properties of the phase transition in a QCD phase diagram.

DOI: 10.1103/PhysRevLett.122.061101

Introduction.—The 2017 detection of gravitational waves (GWs) from a binary neutron-star merger event GW170817 [1] has opened a new window to study the interior of neutron-stars and, consequently, matter at nuclear densities. This detection alone has already provided important progress in our understanding of the maximum mass of neutron-stars and on the expected distribution in radii and tidal deformabilities [2–8]. In addition, information about the merger product itself has allowed a completely new insight into matter at densities *and* temperatures never observed or produced in a laboratory before. To describe such environments, it is essential to employ a microscopic model of strongly interacting matter that contains the expected degrees of freedom and symmetries to be present under those conditions. For this reason, we present here neutron-star merger simulations using an equation of state (EOS) that contains not only thermal effects but, most importantly, a description in which the degrees of freedom change with density and temperature, going from nucleons to hyperons and, finally, quarks.

This is substantially different from what has been done in previous works, where either only the appearance of hyperons was investigated [9,10], quarks were modeled within a hybrid EOS (with the simple MIT bag model) at zero temperature [11], or only quarks were accounted for (again with the MIT bag model) including temperature effects, but without a hadronic matter component or a crust [12] and, hence, without a phase transition (PT). Furthermore, the last two approaches were based on a conformally flat approximation of general relativity and evolved matter within a smooth particle hydrodynamics approach. In contrast, in this Letter we report on the first simulations employing a self-consistent nuclear EOS including finite-temperature effects and allowing for a first-order PT from hadrons to quarks, together with a covariant general-relativistic description of hydrodynamics coupled to a fully general-relativistic spacetime evolution.

Methods and setup.—Matter in the inner core of neutron-stars is very dense but still strongly interacting. For this reason, although the relevant degrees of freedom in these conditions are expected to be quarks, first-principles theories, such as perturbative QCD, cannot be applied directly. An alternative is to rely on effective models, which can be calibrated to work in the required regime of energies. Here, we choose the Chiral Mean Field (CMF) model, based on a nonlinear realization of the SU(3) sigma model [13]. This is an effective quantum-relativistic model that describes hadrons and quarks interacting via meson exchange and is constructed in a chirally invariant manner, since the particle masses originate from interactions with the medium

and, therefore, decrease at high densities or temperatures. The model is in agreement with standard nuclear and astrophysical constraints [14,15], as well as lattice QCD and perturbative QCD [16,17]. In particular, in the limit of zero-temperature, zero-angular momentum, it predicts a maximum mass of 2.07 $M_\odot$ for an hadronic star (1.97 $M_\odot$ when quarks are included) and a radius of 13.7 km for a reference star of 1.4 $M_\odot$.

This approach allows for the existence of soluted quarks in the hadronic phase and soluted hadrons in the quark phase at finite temperature. However, quarks or hadrons will always give the dominant contribution in the quark-hadron phase, and the two phases can be distinguished through their order parameters. This interpenetration of quarks and hadrons (that increases with temperature) provides a physically effective description and is indeed required to achieve the crossover transition known to take place at small chemical potential values [18]. While this approach is suitable to describe matter in the neutron-star core, another description is needed for the crust and the very low density regions produced in binary mergers. For these, we have matched the CMF EOS to the nuclear statistical equilibrium description presented in Ref. [19].

To describe the evolution of the merging system, we solve the coupled Einstein-hydrodynamics system [20] using the newly developed FRANKFURT/ILLINOISGRMHD code (FIL), which is a high-order extension of the publicly available ILLINOISGRMHD code [21], part of the EINSTEIN TOOLKIT [22]. In particular, FIL, which belongs to the family of Frankfurt relativistic-astrophysics codes FRAC), implements a fourth-order accurate conservative finite-difference scheme [23] using a WENO-Z reconstruction [24], coupled to a Haarten-van-Leer-Lax-Einfeldt Riemann solver [25]. The code handles temperature-dependent EOSs utilizing a novel infrastructure, and the conversion from conservative to primitive variables follows [26] for purely hydrodynamical simulations. To account for weak interactions, a neutrino-leakage scheme is implemented following Refs. [27–29]. The FIL code can also handle neutrino heating via an $M0$ scheme [30] and has recently participated in a multigroup code comparison demonstrating its ability to provide an accurate and fully convergent description of the dynamics of merging compact stars. We will comment further on the its capabilities in an upcoming publication.

The spacetime is evolved using the $Z4c$ formulation of the Einstein equations [31], which is a conformal variant of the $Z4$ family [32] (see also Ref. [33]), following the setup in Ref. [34], while the gauges are the same as in Refs. [35,36]. The initial data are modeled under the assumption of irrotational quasicircular equilibrium [37] and are computed by the LORENE library. The binaries are initially at a distance of 45 km and perform around five orbits before the merger. The numerical grid uses the fixed-mesh refinement driver CARPET [38], with a total of seven refinement levels having a highest resolution of $\simeq$250 m covering the two stars and a total extent of $\simeq$1500 km.

Results.—While we have evolved a larger spectrum in masses for binaries with either equal or unequal masses, we next concentrate on two cases that best illustrate the onset of a first-order PT. These are equal-mass binaries with total masses $M = 2.8\ M_\odot$ and $2.9\ M_\odot$, hereafter referred to as the low- and high-mass binaries, respectively. Lower-mass binaries lead to postmerger objects with zero or minute quark fraction, while higher-mass binaries collapse to a black hole before a PT can fully develop. As anticipated above, a distinctive feature of our approach is the ability to cleanly and robustly determine the role of quarks in the merger remnant by using the same EOS with and without quarks. Because of this, for each of the two masses we perform two identical simulations employing either the standard CMF EOS where quarks and a strong first-order PT are included (i.e., CMF_Q) or a purely hadronic version in which the quarks are not included (i.e., CMF_H). In the case of the high-mass, CMF_Q binary, we have also performed a simulation with a very high resolution of $\simeq$125 m. Leading only to a 1.5% difference in the collapse time, this confirms that the reference resolution reported here is sufficient to capture qualitatively the dynamics of the PT.

We begin by describing the overall evolution during and after the merger of the low-mass binary with total mass $M = 2.8\ M_\odot$. In particular, Fig. 1 reports three representative snapshots on the equatorial plane. Right after the merger time t_{mer}, and slightly before the time shown in the left-hand panel of Fig. 1, the regions with high temperatures are near the central regions of the hypermassive neutron-star (HMNS). Some time later, and in analogy with what was shown in previous studies [35,39], the temperature distribution shows two "hot spots" in spatially opposite regions (middle panel) that also correspond to local minima of the number density (see Ref. [35] for a detailed discussion in terms of the Bernoulli constant). Interestingly, already a few milliseconds after the merger, a small but nonzero amount of quarks constituting $\lesssim$0.02% of the total baryon mass begins to appear in regions of high temperature and *before* a first-order PT occurs. Because even small fractions of quarks can alter the pressure, the quadrupole moment of the HMNS will be different when compared to the pure hadronic case. As time progresses, the hot spots merge into a ring (right-hand panel), at which time also the density has reached the critical value for the onset of the PT, leading to the production of a large amount of quarks in the core of the HMNS. When this happens, the quark fraction Y_{quark} can be as large as 0.9 locally and quarks represent $\sim$15%–20% of the total baryon mass.

The onset of the PT has a dramatic effect on the equilibrium of the HMNS. The very rapid softening of the EOS, in fact, leads to a rapid compression of the central region of the HMNS; the resulting release of gravitational binding energy produces a sharp increase in the baryon number density and a massive heat up of the core that, in the absence of the PT, would be cold.

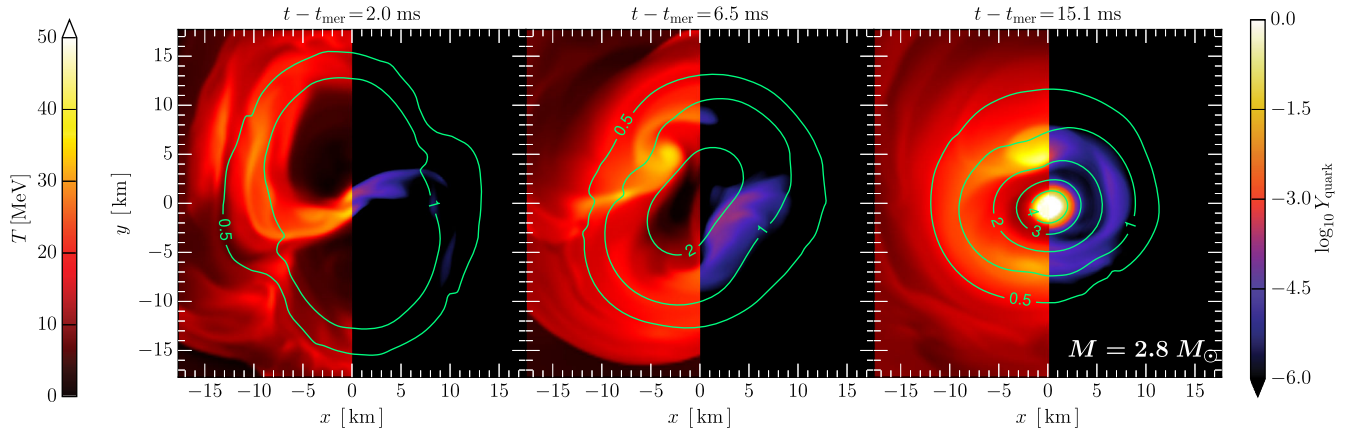

FIG. 1. Snapshots on the equatorial plane at three representative times of the evolution of the low-mass binary. For each snapshot, the left-hand part of the panel reports the temperature T, while the right-hand part reports the quark fraction $Y_{\rm quark}$. The green lines show contours of constant number baryon density in units of the nuclear saturation density $n_{\rm sat}$. Note that a PT takes place only shortly before the HMNS collapses to a black hole (cf. right-hand panel).

To appreciate this better, Fig. 2 shows the same quantities as Fig. 1, but in the meridional plane for the high-mass binary and after the PT has taken place. Different panels compare simulations performed with the CMF$_Q$ EOS, where quarks are present (top panels) with simulations employing the CMF$_H$ EOS, in which quarks are suppressed (bottom panels). It is remarkable to note the large quark fraction in the center and also in regions of high temperature (top right-hand panel), which is, of course, absent for the CMF$_H$ EOS (bottom right-hand panel). Similarly, while the temperature distributions are very similar in the outer parts of the HMNS, where the densities are comparatively low, they are very different in the inner regions.

Finally, it should be emphasized that the CMF$_Q$ EOS does not lead to the formation of a gravitationally stable quark phase and, therefore, the very massive quark core collapses essentially in free fall, i.e., in $\lesssim$1 ms, to a rotating black hole. As discussed in Ref. [40], a relaxation of the charge-neutrality constraint in the EOS from being local to being global (a so-called Gibbs construction) would create a stable mixture of phases that, in the case of massive and isolated stars, would extend to several kilometers within the star. We here do not relax such constraint as we are interested in studying the effect of a steep first-order PT and thus in finding the most extreme signals that could be produced in such events.

Since the deconfinement of quarks depends on both the density and the temperature of matter, it is interesting to consider which regions of the EOS are actually probed by the merger remnant. Hence, in close analogy with what is done in heavy-ion collisions [41], Fig. 3 shows the evolution of the maximum baryon number density $n_{\rm max}$ (normalized to the nuclear saturation density $n_{\rm sat}$) and of the maximum temperature $T_{\rm max}$ for the low-mass binary evolved with the CMF$_Q$ EOS. The time series spans a time between 5 and 15 ms after merger. In essence, diamonds refer to the part of the matter in the core of the HMNS, while circles illustrate the conditions in the hot and low-density regions affecting the quadrupole moment. Note that matter in the HMNS core exhibits higher densities of $>2n_{\rm sat}$, but also temperatures below 10 MeV; by contrast, heavy-ion collisions of, e.g., Au + Au at energies of $\sim$0.5–1 GeV, probe number densities above $n_{\rm sat}$ and temperatures of $50 \lesssim T/{\rm MeV} \lesssim 100$ (not shown in Fig. 3).

Loss of angular momentum through GWs leads to a continuous rise of the central density (hence, of $n_{\rm max}/n_{\rm sat}$), which ultimately reaches the boundary of the first-order PT (gray shaded area) in Fig. 3 at $\sim$13 ms after merger. While contracting, the core of the HMNS crosses this region very rapidly and establishes an almost-pure quark phase heated up to temperatures >40 MeV. If metastable, this core might influence the surrounding material, although the densities inside the HMNS are so high that neutrinos are

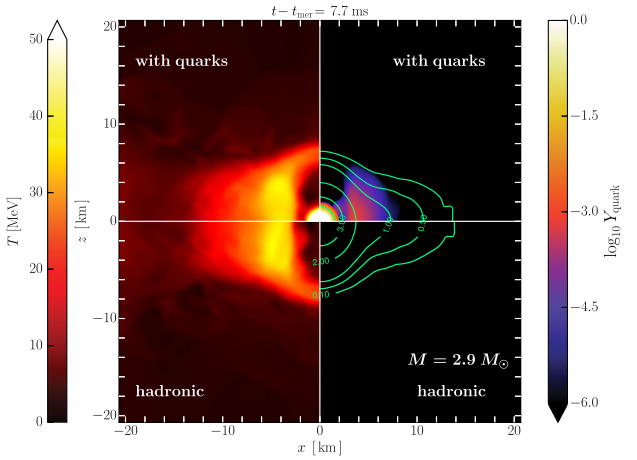

FIG. 2. Same as Fig. 1 but on the meridional plane. The top (bottom) panels show simulations with the CMF$_Q$ (CMF$_H$) EOSs. The snapshot refers to the high-mass binary at a time shortly before the collapse to a black hole.

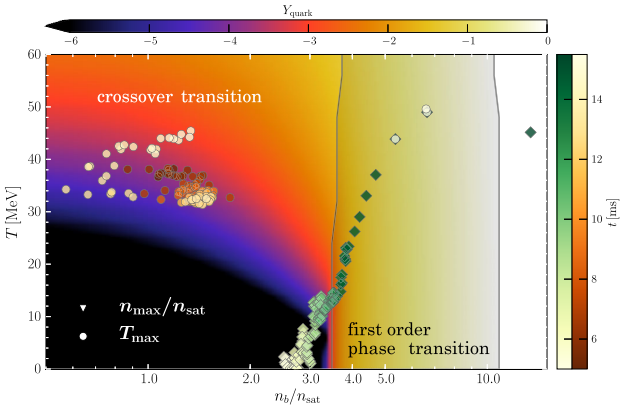

FIG. 3. Evolution of the maximum normalized baryon number density (diamonds) and temperature (circles) after the merger for the low-mass binary with the CMF_Q EOS. Different times of the evolution are represented with a color code, together with the quark fraction $Y_{\rm quark}$. The gray shaded area shows the first-order PT region.

essentially trapped. As can be seen from the last marker of the density evolution in Fig. 3, the HMNS core undergoes a complete PT to quarks and the whole HMNS collapses immediately after the PT. Note that the region of highest temperature is initially at densities smaller than $\sim n_{\rm sat}$, but the temperature is sufficiently high for quarks to appear in small amounts. After the HMNS core crosses the PT boundary, the maximum temperature rises steeply and thus the fluid elements with maximum density and temperature coincide.

We complete our discussion of the PT by considering its signatures on the GW emission by means of the strain, frequency, and phase difference, which are reported in Fig. 4 for the low- and high-mass binary. Note that because the densities and temperatures during the inspiral are too small to cause the formation of quarks, the GW signal is identical for the two EOSs and for both masses. This is radically different from what happens when comparing merger simulations using EOSs with and without hyperons, as these show differences in the GW signal already during the inspiral [9,10], due to the softening caused by the presence of hyperons. For such EOSs, a dephasing is thus *always* present, both during the inspiral and after the merger, since there are always portions of the stars with intrinsically different EOSs. In our case, instead, it is only *after* the merger that differences arise due to the presence of quarks.

For the low-mass binary, and after ∼5 ms from the merger, the GWs from the remnants start to show a linear dephasing that reaches about 3 rad by the time the binary with the CMF_Q EOS collapses to a black hole (bottom left-hand panel). The start of the phase difference, which is essentially zero even after the merger, coincides with the formation of the two hot spots and, thus, with the appearance of quarks. In fact, although $Y_{\rm quark}$ is very small at those times, it is sufficient to produce changes in the pressure of ∼5%, that are responsible for the changes in the GW emission, both in amplitude and in frequency (top left-hand panel), thus producing a mismatch between two postmerger spectra [42–47]. These changes in pressure also lead to a small damping of the GW amplitude prior to collapse, which is triggered by the first-order PT for the CMF_Q EOS. Hence, the lifetime of the HMNS is shorter than in the purely hadronic case.

In many respects, the left-hand panels of Fig. 4 are a representative example of the signatures of a PT in a binary merger. In an idealized scenario where the GW signal from the inspiral is measured with great precision and can be associated with confidence to a purely hadronic EOS (the inspiral can only probe comparatively low-density regions of the EOS), the unexpected dephasing of the template-matched postmerger signal [48,49], together with the anticipated collapse of the HMNS, would provide evidence that a PT at several times $n_{\rm sat}$, possibly of the type described here, has taken place in its core. Of course, a single detection

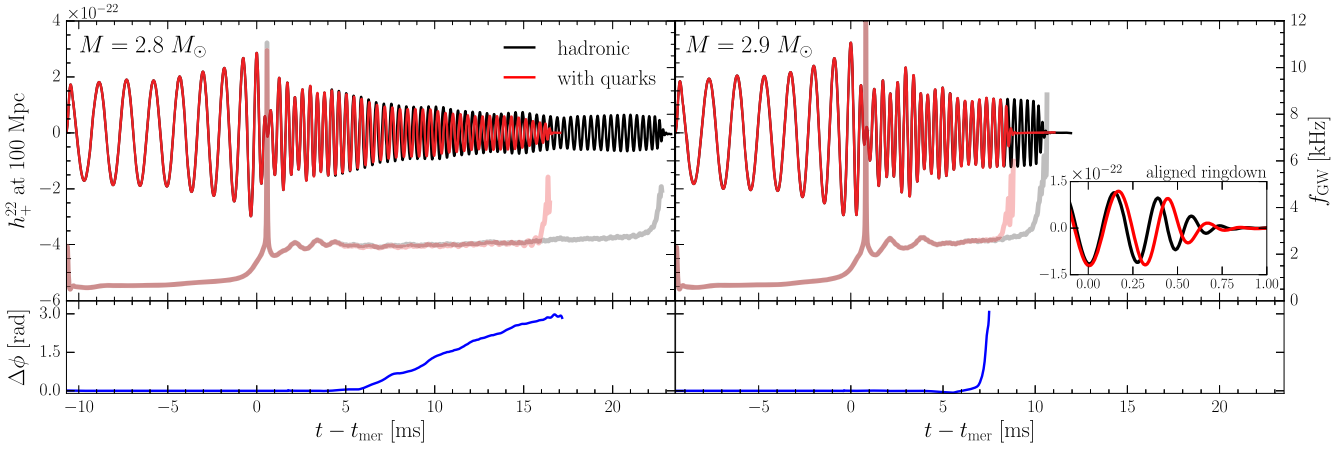

FIG. 4. Properties of the GW emission for the low- (left-hand panels) and high-mass binaries (right-hand panels). The top panels report the strain h_+^{22} for the two EOSs, together with the instantaneous GW frequency $f_{\rm GW}$ (semitransparent lines). The bottom panels show the phase difference $\Delta\Phi$ between the two signals. The inset in the top right-hand panel highlights the differences in the ringdown.

could still be accommodated via a tweaking of the EOS in the high-density part of a hadronic EOS. However, the "tweaking" would be increasingly hard with multiple detections as it cannot describe the complex nonlinear occurrence of the PT.

The right-hand panels of Fig. 4 report the properties of the GW signal for the high-mass binaries, both of which collapse very rapidly for EOSs with and without quarks. The differences in this case are harder to detect since the dephasing starts only after $\sim$5 ms, but is very quickly suppressed by the collapsing signal. The latter, however, is different, as shown in the small inset in the top right-hand panel of Fig. 4, where the two ringdown signals are suitably aligned. These differences are caused by distinct free-fall times of the cores of the HMNSs, which are shorter in the case of the ultrasoftened EOS with quarks. Although these differences are not large (the relative difference in the ringdown frequency is $\lesssim$25%, yielding an overlap of only $\mathcal{O} = 0.92$ [50,51]), they are large enough to be distinguishable if detected by third-generation GW detectors [52,53]. As a final remark, we point out that all of the dynamics reported above are found also when simulating unequal-mass binaries with mass ratio $q = 0.8$; the main difference in this case is that the PT occurs off-center because the high-density region is also off-centered.

Conclusions.—We have presented the first fully general-relativistic simulations of merging binary neutron-stars including quarks at finite temperatures. Because in our approach the presence of quarks can be turned off consistently, it was possible to study their imprint on the merger in a clean and robust manner. Moreover, since our description allows for the appearance of small amounts of quarks below the PT region related to the crossover transition at low densities, we were able to observe significant nonzero quark fractions in regions of high temperature but densities below saturation. The changes in pressure produced by these soluted quarks were shown to lead to a systematic dephasing *only* of the postmerger GW emission, which, if accumulated over several milliseconds, can produce a decisive signature in the postmerger GW signal and spectrum. This behavior is markedly different from that of other hyperonic EOSs, which show softenings already during the inspiral. Furthermore, the inclusion of a first-order PT in a thermodynamically consistent way has allowed us to associate the PT with the formation of a very hot and ultradense quark core in the HMNS, that was gravitationally unstable and collapsed to a black hole. Finally, despite the short lifetime of the quark phase, we have shown that its collapse, which proceeds essentially in free fall, leads to different black-hole ringdown frequencies, another useful signature of the occurrence of the PT.

The work presented here can be extended in at least three ways. Firstly, this can be done by considering an EOS that would allow for the existence of a metastable quark core after a PT. In this case, the postmerger GW spectrum would be the combination of the spectrum of the purely hadronic remnant together with that produced after the PT. Secondly, a PT to a metastable quark core in the HMNS could lead (either immediately or after a diffusion timescale) to a burst signal in neutrinos in analogy with what was suggested for supernovae [54,55], providing yet another evidence of the PT. Finally, the occurrence of the PT will also impact the spectral properties of the postmerger signal to the point that the f_2 oscillation frequency may exhibit a jump to higher frequency as a result of the PT to a different metastable HMNS [56,57]. These scenarios will be explored in future works.

We thank M. Alford, T. Galatyuk, J. Schaffner-Bielich, J. Steinheimer, and J. Stroth for useful discussions. Support comes also in part from "PHAROS," COST Action CA16214; LOEWE-Program in HIC for FAIR; European Union's Horizon 2020 Research and Innovation Programme (Grant No. 671698) (call FETHPC-1-2014, project ExaHyPE); the ERC Synergy Grant "BlackHoleCam: Imaging the Event Horizon of Black Holes" (Grant No. 610058); and by the National Science Foundation under Grant No. PHY-1748621. The simulations were performed on the SuperMUC cluster at the LRZ in Garching, on the LOEWE cluster in CSC in Frankfurt, and on the HazelHen cluster at the HLRS in Stuttgart.

Note added in the proof.—Recently, Ref. [58] has studied the impact of a first-order phase transition taking place directly at merger. Although no waveforms are presented in [58], we expect differences to be present already in the inspiral as they are visibile in the maximum density.

[1] B. P. Abbott *et al.* (LIGO Scientific Collaboration and Virgo Collaboration), Phys. Rev. Lett. **119**, 161101 (2017).
[2] E. Annala, T. Gorda, A. Kurkela, and A. Vuorinen, Phys. Rev. Lett. **120**, 172703 (2018).
[3] B. Margalit and B. D. Metzger, Astrophys. J. Lett. **850**, L19 (2017).
[4] L. Rezzolla, E. R. Most, and L. R. Weih, Astrophys. J. Lett. **852**, L25 (2018).
[5] D. Radice, Astrophys. J. Lett. **838**, L2 (2017).
[6] M. Ruiz, S. L. Shapiro, and A. Tsokaros, Phys. Rev. D **97**, 021501 (2018).
[7] M. Shibata, S. Fujibayashi, K. Hotokezaka, K. Kiuchi, K. Kyutoku, Y. Sekiguchi, and M. Tanaka, Phys. Rev. D **96**, 123012 (2017).
[8] E. R. Most, L. R. Weih, L. Rezzolla, and J. Schaffner-Bielich, Phys. Rev. Lett. **120**, 261103 (2018).
[9] Y. Sekiguchi, K. Kiuchi, K. Kyutoku, and M. Shibata, Phys. Rev. Lett. **107**, 211101 (2011).
[10] D. Radice, S. Bernuzzi, W. Del Pozzo, L. F. Roberts, and C. D. Ott, Astrophys. J. Lett. **842**, L10 (2017).
[11] R. Oechslin, K. Uryu, G. S. Poghosyan, and F. K. Thielemann, Mon. Not. R. Astron. Soc. **349**, 1469 (2004).

[12] A. Bauswein, R. Oechslin, and H.-T. Janka, Phys. Rev. D **81**, 024012 (2010).
[13] P. Papazoglou, D. Zschiesche, S. Schramm, J. Schaffner-Bielich, H. Stoecker, and W. Greiner, Phys. Rev. C **59**, 411 (1999).
[14] V. Dexheimer and S. Schramm, Astrophys. J. **683**, 943 (2008).
[15] R. Negreiros, V. A. Dexheimer, and S. Schramm, Phys. Rev. C **82**, 035803 (2010).
[16] V. A. Dexheimer and S. Schramm, Phys. Rev. C **81**, 045201 (2010).
[17] J. Roark and V. Dexheimer, Phys. Rev. C **98**, 055805 (2018).
[18] Y. Aoki, G. Endrodi, Z. Fodor, S. D. Katz, and K. K. Szabo, Nature (London) **443**, 675 (2006).
[19] A. da Silva Schneider, L. F. Roberts, and C. D. Ott, Phys. Rev. C **96**, 065802 (2017).
[20] L. Rezzolla and O. Zanotti, *Relativistic Hydrodynamics* (Oxford University Press, Oxford, 2013).
[21] Z. B. Etienne, V. Paschalidis, R. Haas, P. Mösta, and S. L. Shapiro, Classical Quantum Gravity **32**, 175009 (2015).
[22] F. Löffler, J. Faber, E. Bentivegna, T. Bode, P. Diener, R. Haas, I. Hinder, B. C. Mundim, C. D. Ott, E. Schnetter, G. Allen, M. Campanelli, and P. Laguna, Classical Quantum Gravity **29**, 115001 (2012).
[23] L. Del Zanna, O. Zanotti, N. Bucciantini, and P. Londrillo, Astron. Astrophys. **473**, 11 (2007).
[24] R. Borges, M. Carmona, B. Costa, and W. Don, J. Comput. Phys. **227**, 3191 (2008).
[25] A. Harten, P. D. Lax, and B. van Leer, SIAM Rev. **25**, 35 (1983).
[26] F. Galeazzi, W. Kastaun, L. Rezzolla, and J. A. Font, Phys. Rev. D **88**, 064009 (2013).
[27] M. Ruffert, H.-T. Janka, and G. Schaefer, Astron. Astrophys. **311**, 532 (1996).
[28] S. Rosswog and M. Liebendörfer,Mon. Not. R. Astron. Soc. **342**, 673 (2003).
[29] E. O'Connor and C. D. Ott, Classical Quantum Gravity **27**, 114103 (2010).
[30] D. Radice, F. Galeazzi, J. Lippuner, L. F. Roberts, C. D. Ott, and L. Rezzolla, Mon. Not. R. Astron. Soc. **460**, 3255 (2016).
[31] S. Bernuzzi and D. Hilditch, Phys. Rev. D **81**, 084003 (2010).
[32] C. Bona, T. Ledvinka, C. Palenzuela, and M. Zácek, Phys. Rev. D **67**, 104005 (2003).
[33] D. Alic, C. Bona-Casas, C. Bona, L. Rezzolla, and C. Palenzuela, Phys. Rev. D **85**, 064040 (2012).
[34] D. Hilditch, S. Bernuzzi, M. Thierfelder, Z. Cao, W. Tichy, and B. Brügmann, Phys. Rev. D **88**, 084057 (2013).
[35] M. Hanauske, K. Takami, L. Bovard, L. Rezzolla, J. A. Font, F. Galeazzi, and H. Stöcker, Phys. Rev. D **96**, 043004 (2017).
[36] L. Bovard, D. Martin, F. Guercilena, A. Arcones, L. Rezzolla, and O. Korobkin, Phys. Rev. D **96**, 124005 (2017).
[37] E. Gourgoulhon, P. Grandclément, K. Taniguchi, J.-A. Marck, and S. Bonazzola, Phys. Rev. D **63**, 064029 (2001).
[38] E. Schnetter, S. H. Hawley, and I. Hawke, Classical Quantum Gravity **21**, 1465 (2004).
[39] W. Kastaun, R. Ciolfi, and B. Giacomazzo, Phys. Rev. D **94**, 044060 (2016).
[40] M. Hempel, V. Dexheimer, S. Schramm, and I. Iosilevskiy, Phys. Rev. C **88**, 014906 (2013).
[41] P. Foka and M. A. Janik, Rev. Phys. **1**, 154 (2016).
[42] A. Bauswein and H.-T. Janka, Phys. Rev. Lett. **108**, 011101 (2012).
[43] N. Stergioulas, A. Bauswein, K. Zagkouris, and H.-T. Janka, Mon. Not. R. Astron. Soc. **418**, 427 (2011).
[44] K. Takami, L. Rezzolla, and L. Baiotti, Phys. Rev. Lett. **113**, 091104 (2014).
[45] K. Takami, L. Rezzolla, and L. Baiotti, Phys. Rev. D **91**, 064001 (2015).
[46] S. Bernuzzi, T. Dietrich, and A. Nagar, Phys. Rev. Lett. **115**, 091101 (2015).
[47] L. Rezzolla and K. Takami, Phys. Rev. D **93**, 124051 (2016).
[48] S. Bose, K. Chakravarti, L. Rezzolla, B. S. Sathyaprakash, and K. Takami, Phys. Rev. Lett. **120**, 031102 (2018).
[49] K. Chatziioannou, J. A. Clark, A. Bauswein, M. Millhouse, T. B. Littenberg, and N. Cornish, Phys. Rev. D **96**, 124035 (2017).
[50] L. Lindblom, B. J. Owen, and D. A. Brown, Phys. Rev. D **78**, 124020 (2008).
[51] B. Giacomazzo, L. Rezzolla, and L. Baiotti, Mon. Not. R. Astron. Soc. **399**, L164 (2009).
[52] M. Punturo *et al.*, Classical Quantum Gravity **27**, 084007 (2010).
[53] B. P. Abbott *et al.* (LIGO Scientific Collaboration), Classical Quantum Gravity **34**, 044001 (2017).
[54] I. Sagert, T. Fischer, M. Hempel, G. Pagliara, J. Schaffner-Bielich, A. Mezzacappa, F.-K. Thielemann, and M. Liebendörfer, Phys. Rev. Lett. **102**, 081101 (2009).
[55] T. Fischer, N.-U. F. Bastian, M.-R. Wu, S. Typel, T. Klähn, and D. B. Blaschke, Nat. Astron. **2**, 980 (2018).
[56] M. Hanauske, J. Steinheimer, L. Bovard, A. Mukherjee, S. Schramm, K. Takami, J. Papenfort, N. Wechselberger, L. Rezzolla, and H. Stöcker, J. Phys. Conf. Ser. **878**, 012031 (2017).
[57] M. Hanauske, Z. S. Yilmaz, C. Mitropoulos, L. Rezzolla, and H. Stöcker, EPJ Web Conf. **171**, 20004 (2018).
[58] A. Bauswein, N.-U. F. Bastian, D. B. Blaschke, K. Chatziioannou, J. A. Clark, T. Fischer, and M. Oertel, following Letter, Phys. Rev. Lett. **122**, 061102 (2019).